Published in final edited form as:
Nano Lett. 2008 November ; 8(11): 3953–3958. doi:10.1021/nl802442x.

Quantum dots as multimodal photoacoustic and photothermal contrast agents

Evgeny V. Shashkov[1,2], **Maaike Everts**[3], **Ekaterina I. Galanzha**[1,4], and **Vladimir P. Zharov**[1]

1 *Philips Classic Laser Laboratories, University of Arkansas for Medical Sciences (UAMS), Little Rock, AR 72205*

2 *Prokhorov General Physics Institute, Moscow, 119991, Russia*

3 *Division of Human Gene Therapy, University of Alabama at Birmingham, Birmingham, AL 35294*

4*I nstitute of Optics and Biophotonics, Saratov State University, Saratov, 410012 Russia*

Abstract

Quantum dots (QDs) have primarily been developed as fluorescent probes with unique optical properties. We herein demonstrate an extension of these QD utilities to photoacoustic (PA) and photothermal (PT) microscopy, using a nanosecond pulse laser excitation (420–900 nm, 8 ns, 10^{-3}-10 J/cm^2). The laser-induced PA, PT and accompanying bubble formation phenomena were studied with an advanced multifunctional microscope, which integrates fluorescence, PA, PT imaging, and PT thermolens modules. It was demonstrated that QDs, in addition to being excellent fluorescent probes, can be used as PA and PT contrast agents and sensitizers, thereby providing an opportunity for multimodal PA-PT-fluorescent imaging as well as PT therapy. Further improvements for this technology are suggested by increasing the conversion of laser energy in PT, PA, and bubble phenomena in hybrid multilayer QDs that have optimized absorption, thermal, and acoustic properties.

Quantum dots (QDs) are emerging as an exciting new class of nanoparticles with many biomedical applications, including non-invasive *in vivo* imaging of tumors, lymph nodes, vascular beds and cellular trafficking (1,2, and references therein). QDs were first and foremost developed as fluorescent probes with unique optical properties, such as relatively high quantum yields (up to 20–40%), broad excitation (i.e., absorption) spectra ranging from ultraviolet (UV; 400 nm) to near-infrared (NIR; 750 nm), and relatively narrow emission spectra (40–80 nm width). Nevertheless, because of the still limited quantum yield, most absorbed light energy is eventually converted into heat through several nonradiative relaxation pathways. This suggests a potential use of photothermal (PT) methods to study QD properties 3,4. In addition, a recently developed highly sensitive photoacoustic (PA) flow cytometry demonstrated the capability to, *in vivo*, detect single cancer cells and bacteria labeled with absorbing nanoparticles as well as with conventional NIR fluorescent organic dyes such as Indocyane Green (ICG) 5,6. Herein we demonstrate for the first time that QDs can also be considered excellent PA agents, thereby further advancing this rapid PA spectroscopy-microscopy-cytometry, using nanosecond pulse lasers. This is especially true upon integration with time-resolved PA-PT-fluorescent diagnostic techniques, thereby demonstrating that QDs have the potential to be used as sensitizers for PT therapy guided by PA, PT and fluorescent imaging.

When QDs are irradiated by short laser pulses, multi-excitation relaxation processes in the nanoparticles lead eventually to conversion of part of the absorbed energy into heat and subsequent PA effects (Fig. 1). To provide effective generation of PA signals from individual QDs, the physical processes responsible for PA effects (optical excitation →nonradiative relaxation→heating→acoustic wave generation) should meet several conditions referred to as

'confinements', which depend on QD and laser parameters. The core-shell CdSe/ZnS QDs have a relatively high absorption cross-section in the visible and NIR range (typically σ_{QD}~10^{-14}-10^{-15} cm^2), which exceeds that of the best NIR fluorophores (e.g., σ_B ~10^{-16} cm^2 for ICG) and endogenous cellular background (10^{-17} -10^{-18} cm^2) 4,7–9. This difference in absorption cross-sections between the QDs and the background provides excellent *optical confinement* (i.e. $\sigma_{QD} \gg \sigma_B$). When QDs are excited with a sufficiently high laser fluence in nanosecond pulse mode, multi-excitation (or at least bi-excitation) leads to the creation of multi-excitons with a rapid picosecond non-radiative relaxation time (τ_{NR}) to the band-edge state and hence into the development of heat. This rapid picosecond-scale relaxation time 4, compared to the longer nanosecond-scale radiative relaxation time (τ_R) that is responsible for fluorescence, provides the *relaxation confinement* ($\tau_{NR} \leq \tau_R$). The *quantum confinement* is related to the quantum size localization energy and strong electron-photon interactions in QDs (e.g. the blue shift of the absorption edge with decreasing QD size below the de Broglies's wavelength of the electron) 1,2. To provide efficient QD heating with negligible heat diffusion effects, the laser pulse width (t_P) should be less than the thermal relaxation time (τ_T), i.e, $t_p \leq \tau_T$, constituting the *thermal confinement*3,8,9. For spherical QDs with radius R, $\tau_T = R^2/6.75k$, where k is thermal diffusivity (e.g., for R=20 nm and k = 1.44×10^{-3} cm^2/sec [for water medium], τ_T ~1 ns). The efficient transformation of thermal energy into acoustic energy occurs at $t_P \leq \tau_A = 2R/c_s$ (the *acoustic confinement*) 6,9, where τ_A is the transit time of the acoustic wave traveling through QDs and c_s is the speed of sound. For R=10 nm and less, and water with $c_s = 1.5\times 10^5$ cm/sec, t_P is thus in the sub-nanosecond ranges.

Experimental schematics

Laser-induced PT and accompanying PA and bubble formation phenomena in QDs were evaluated using integrated PT/PA schematics (Fig. 2) on the technical platform of an Olympus BX51 microscope (Olympus America, Inc.), with parameters described elsewhere 6,8. In short, either single or many QDs in either a thin (≤1μm) or thick (120 μm) suspension layer on microscope coverslips were irradiated with a pump laser pulse (wavelength 420 – 2,300 nm; pulse width 8 ns; fluence 0.001 – 10 J/cm^2) (Lotis Ltd., Minsk, Belarus). In PT thermolens mode, laser-induced temperature-dependent refractive index variations in the samples resulted in defocusing of the collinear CW He-Ne laser probe beam (633 nm, 1.4 mW; model 117A, Spectra-Physics, Inc.), which was detected as an integral PT response by a photodiode (C5658; Hamamatsu Corp.) with a pinhole and a TDS 3032B oscilloscope. In PT imaging (PTI) mode, the refractive index variations leading to phase and local thermolens effects of a second, collinear laser probe pulse (Raman shifter 639 nm; pulse width 12 ns; pulse energy 2 nJ) were imaged with a AE-260E CCD camera (512×512 pixels and pixel size of 20 μm (Apogee Inc., Santa Monica, CA) and analyzed with customized software 8. The diameters of pump- and probe-beam spots in the sample plane were in the range of 20–30 μm and 10–15 μm, respectively. PA waves (referred further as PA signals) were detected by an ultrasound transducer (model 6528101, 3.5 MHz, 5.5 mm in diameter; Imasonic Inc., Besançon, France), attached to the slide using ultrasound gel for acoustic matching between the transducer and the glass. Signals from the transducer were amplified (amplifier model 5660B, 2 MHz; Panametrics) and recorded with the afore-mentioned oscilloscope.

A fluorescence module with colored CCD cameras (Nikon DXM1200) was added to the integrated system (Fig. 2) to provide fluorescent images of QDs using a conventional lamp with filters. For PA and PT experiments, we used QDs with a polymer coating as well as protein (streptavidin) molecules attached (Qdot 655 Nanocrystals, streptavidin conjugate, Invitrogen, Carlsbad, CA) of around 15–20 nm in diameter (total), with an emission around 655 nm. Initial concentration of QDs (in 50 mM borate buffer, pH 8.3, 1 M betaine, 0.05% sodium azide) was 10^{-9} M/mL (~6 x 10^{14} QDs/mL). To provide either only a few or a multiple of QDs in the laser beam, QDs were diluted using a buffer of 2% BSA/PBS.

PT imaging

The dilution of the sample for the thin slide imaging was chosen to provide the presence of approximately 20–30 QDs in the laser beam. In PTI mode, high resolution PT images demonstrated relatively good absorption contrast of individual QDs in a thin (≤1μm) suspension layer (Fig. 3c), comparable to that of conventional fluorescent images (Fig. 3a). The PT resolution was determined by the microscope objective itself (~0.7 μm at 20×, NA 0.4; ~350 nm at 60×, NA 1.25), without significant influence of thermal blurring of the diffraction spot during the short laser pulse (for t_p = 8 nsec, this blurring is just 69 nm) 8. This capability of far-field PTI to visualize individual nanoscale QDs was based on analysis of laser-induced thermal fields (or microbubbles) around single QDs during their expansion above the diffraction limit due to heat diffusion. It should be noted that the temporal dynamics of local structures in PT images (associated with fast heating and cooling of individual QDs) at different time delays between pump and probe pulses may provide information of their average sizes, as previously described 8.

The PTI contrast increased with increasing pulse energy, which eventually was accompanied by microbubble formation around overheated QDs, especially their small clusters (i.e., closely located QDs) with the appearance of several overlapping microbubbles (Fig. 3d). The bubble –associated strong refraction effects shielded the remained “pure” PT images (i.e., without bubble) of individual QDs.

In PT thermolens linear mode (i.e., without QD photodamage), PT signals from QDs in thick-slide-imaging showed the standard fast rising unipolar peak associated with rapid (ps-ns scale) QD heating, and a slower (μs scale) tail, corresponding to QDs cooling through heat diffusion into the surrounding solution (Fig. 3e). Because many closely located QDs were simultaneously irradiated within the pump laser beam (~20 μm in diameter), the laser-induced heat, which was initially localized in individual QDs, was rapidly (ns scale at high QD concentration) redistributed due to heat diffusion within the laser beam, leading eventually to an increase in cooling time to 30 – 40 μs. This indicates that the cooling time is determined by the laser beam diameter rather than by the size of individual QDs, for which cooling time is much shorter, i.e., nanosecond and sub-nanosecond scale (see above). This is similar to the monitoring of PT effects in the solution of conventional dyes such as ICG or neutral red 5,8 or high concentration carbon nanotubes (CNTs) 10, when a relatively large amount of homogenously distributed absorbing units (i.e., dye molecules or CNTs) molecules appears in the detected volume.

The amplitudes of the PT responses increased with increasing pulse energy until the local temperature around the QDs or their clusters reached the microbubble formation threshold, leading to the appearance of a stronger (5–10 fold) and sharper peak (Fig. 3f) compared to linear PT responses (Fig. 3e) due to bubble-related optical (refraction and scattering) phenomena 8. After the initial expansion, the vapor rapidly cooled and condensed, and the bubbles collapsed. The lifetime of the bubbles, 0.2–4 μsec, depended on the number of QDs in clusters and on the laser energy level. At a high energy level, several microbubbles might arise simultaneously, overlap, and merge with each other (Fig. 3d), leading to further increase of PT signal amplitude with some fluctuations (Fig. 3f) related to different time of nucleation and lifetime of the individual microbubbles.

PA effects

The tendencies observed for PT imaging and PT thermolens signals at different laser energies appeared also in the formation of PA signals. The PA signal from QDs had a initial classic bipolar shape 9 transformed into a pulse train due to reflection and resonance effects (Fig. 3g). An increase in laser energy led to increased PA signals, which were enhanced by bubble formation effects leading to non-regular signal shapes (Fig. 3h). Specifically, the PA signal

amplitude gradually increased with an increase of laser fluence in the linear range of 0.1–1 J/cm^2 (Fig. 4a). Then, a nonlinear increase started at 1.5 J/cm^2 with a more profound PA amplitude enhancement (10–20 times) at relatively high fluences in the range of 3–7 J/cm^2, which was associated with the afore-mentioned microbubble formation phenomena. Saturation of the PA signal was observed at energy fluences above 15 J/cm^2, likely associated with laser-induced destruction of QDs. This was indeed confirmed by the behavior of PA signal amplitudes as a function of laser pulse number at various laser fluences (Fig. 4b). There was no sign of laser-induced alteration of PA signal amplitude and hence absorption QD properties (the PA signal is proportional to coefficient absorption of targets) 3,4,8–11 at relatively low fluence, below 3 J/cm^2. Thus, contrary to fluorescence 1,2, the PT signals did not show any blinking behavior. However, at higher fluences, significant decreases in PA signal amplitudes were observed with an increase in pulse number. In particular, at 12.4 J/cm^2, after the first laser pulse the signal decreased ~2 times and almost disappeared after 10 pulses, confirming the possibility of laser-induced disintegration of QDs likely through melting or thermal-based explosion phenomena 12.

Fluorescent imaging revealed inhibition of fluorescence with an increase in laser energy, up to complete disappearances of emission at high energy (Fig. 3b). It should be noted that this fluorescence inhibition was observed at a relatively low laser pulse energy, around 0.5 J/cm^2, at which there was not yet any sign of PA signal degradation (Fig. 4b). This indicates that the mechanisms responsible for fluorescent degradation and “PA bleaching” may have different origins, for example, related to photochemical and PT-based phenomena, respectively.

PA spectra of QDs obtained with a pulse laser were in relatively good agreement with the conventional absorption spectra obtained in suspension with a high QD concentration (Fig. 5). Both of them contain an absorption peak near 640 nm and 635 nm, respectively, both blue shifted from the emission line. However, compared to the conventional spectra, the width of the PA spectra peak is more narrow, the PA peak is slightly red shifted, and at wavelengths shorter than 570 nm the PA rate of signal increase is more profound with decreasing wavelength. The observed phenomena leading to the “sharpening” of PA spectra near the absorption spectral maximum should be associated with non-linear PT-based enhancement of PA signals around QDs, since overheating is more profound when the laser wavelength corresponds to the QD absorption wavelength.

Replacement of water with ethanol led to an increase in both PT and PA signals from QDs of about 5–7 fold at the same level of laser energy. This is in line with our previous data 10, where we observed that ethanol provides more profound heating and more effective bubble formations in laser pulse mode because of its better thermodynamic parameters compared to water (see below), including higher (~3.5 times) coefficient of thermal expansion. We further found that the PA signals from the coated QDs exceeded PA signals from uncoated QDs by several times, at the same laser parameters (639 nm, 0.5 J/cm 2). According to our previous findings 6, this signal enhancement could be a consequence of various features of the external low-absorbing layers: 1) the layer functions as a thermal insulator, thus providing more effective heat accumulation in the internal core and thus elongating the thermal relaxation time τ_T of QDs (for the core alone the τ_T lies in sub-nanosecond range), for better thermal confinement with an 8-ns laser pulse; 2) it improves acoustic and thermal confinements due to larger nanoparticle size; and 3) due to fast thermal expansion it provides more effective generation of PA waves, especially when overheating of the QD core is accompanied by non-linear phenomena such as nanoparticle melting, explosion, and fragmentation 12. Because bubble formation is the main mechanism of cell damage in laser pulse mode 8,12,13, the demonstrated capability of QDs as a PT sensitizer and “bubble” contrast agent allows an extension of QD applications to PT therapy of cancer cells and infections. When QDs are in close proximity of each other, the

overlapping of micro-or nano-bubbles from individual QDs (Fig. 3d) may enhance therapeutic efficiency 13. Hence, in addition to thermal, acoustic and other confinements as discussed above, we can introduce *bubble confinement*, when the minimal size of bubbles matches to distances between QDs. Laser-induced removal of the protective coating around QDs and/or some disintegration of QD crystals (e.g., through core melting or explosion 12) at increased laser energy may be considered as another potential killing mechanism, since uncoated QDs are associated with increased toxicity 1,2. However, this issue requires further study, including damage localization, and clearance of toxic products from organism.

The obtained results clearly demonstrate the potential of QDs to serve as PT and PA contrast agents using an advanced multimodal PT-PA-fluorescent microscope. The highest absorption sensitivity at the single QD level with high spatial resolution (350 nm) was achieved in the pump-probe time-resolved PTI mode (Fig. 3c), with image contrast comparable to that of fluorescent imaging (Fig. 3a). Of note, the PTI mode provided images of some QDs that did not appear in fluorescent images. These data are in line with results from other groups 4 that indicate that low-intensity fluorescent QDs hold absorption properties that are detectable with the PT technique. The additional advantage of the PTI-mode is its fast image acquisition algorithm (10^{-1} -10^{-4} s, depending on CCD camera speed and laser pulse rate), which requires just one laser pulse with a broad beam diameter (10–30 μm) to create a cell image with a resolution approaching the optical diffraction limit 8. In comparison, conventional image algorithms use time-consuming scanning of a focused laser beam across cells and requires seconds if not minutes to obtain a single cell image 1,2,4.

The minimal number of QDs producing readable signals in PT thermolens or PA modes (Fig. 3e,g) was estimated to be 140 and 290 QDs in the detected (i.e. irradiated) volume, respectively. This was verified by measuring signals of a serial dilution of an initial suspension with a known QD concentration, as provided by the manufacturer. In addition, the number of QDs in the laser beam volume at low QD concentration was estimated by simultaneous fluorescent imaging. According to literature, in most applications the typical number of QDs inside labeled cells is around several hundred and higher, up to 10^4 (1, 2, 4, and references therein). Thus, PT thermolens or PA methods should be able to provide detection of single cells containing ≥300–500 QDs *in vitro* and potentially *in vivo*.

Interestingly, the PA detection limit for QDs alone was worse compared to our recently demonstrated PA detection of a just few gold nanorods or their small clusters 6, which absorb much stronger in NIR range than QDs. Therefore, based on our previous 6,10 and current findings, we further identified several ways to improve the QD detection limit by increasing conversion of laser energy into PT, PA, and bubble formation phenomena. In particular, the PA signal is proportional to the absorbed laser energy transformed through non-radiative relaxation into heat, and then through thermal expansion phenomena into PA waves. More specifically, according to theoretical models 8–12, the PA signal is proportional to laser energy, the absorption cross-section, the coefficient of thermal expansion and inversely proportional to density and heat capacity. In addition, bubble formation, as a PA signal enhancer and cell killer, is more effective at a low boiling point and vaporization heat. Thus, the proposed technology has a great potential for further the improvement by optimization of all these parameters.

First, an increase in sensitivity could be achievable by decreasing the laser pulse duration to the picosecond territory, which would match better to the thermal and, especially, acoustic confinements, since the thermal τ_T and acoustic τ_A relaxation times lie in the sub-nanosecond range (see above). Alternatively, the QD relaxation times could be increased by using larger QDs ($\tau_T \sim R^2$, $\tau_A \sim R$), or by providing conditions for self-assembly of QDs into clusters, in which overlapping of laser-induced optical, thermal, acoustic and bubble formation

phenomena will lead to synergistic enhancement of PT and PA cooperative effects 10,13. The formation of QD clusters that have increased average sizes compared to single QDs would allow the use of nanosecond lasers, broadly used in medicine because they are simpler, less expensive, and less harmful for healthy biotissue than picosecond and femtosecond lasers.

To improve PA sensitivity we also propose to: 1) increase absorbed energy through conjugation of relatively low absorbing but highly fluorescent QDs to strongly absorbing nanostructures, both non-fluorescent or fluorescent (e.g., CNTs, gold nanoparticles, or even conventional dyes such as ICG); 2) use insulating layers around QDs or between the QD core and the protective coating that must have low heat diffusion and thus should improve the thermal confinement; and 3) use a layer with a high coefficient of thermal expansion (as is the case for ethanol, 10) and lower speed of sound (as is the case for rubber-like materials), to improve the acoustic confinement. The combination of QDs with gold nanoparticles with various modifications may significantly enhance PA diagnostics and PT nanotherapy, including the development of integrated QD-gold nanoprobes, analogous to gold-CNT complexes that serve as PT contrast agents 13. It should be noted that empty nanostructures like CNTs have a lower heat capacity compared to solid nanoparticles (like carbon or graphite), allowing better heating in pulse mode even with the same absorption properties (see above). In the case of combinations with gold, an increase of QD absorption can be achieved by either synthesizing QDs with thin gold layers, or “labeling” QDs with bioconjugated gold nanoparticles of different compositions and shapes. Gold nanoparticles are able to quench QD photoluminescence 14, and thus increase the efficiency of the transformation of absorbed laser energy into heat, although the quenching effect should be used with precaution if the fluorescent properties of QD are needed. As we have demonstrated previously 11, the absorbed energy, and hence the PA signals can be enhanced in medium with multiphoton absorption of pulse radiation. This mode can also be realized in QDs, exhibiting two-and multiphoton effects 15,16.

PA spectroscopy revealed (Fig. 5) that the optimal spectral range with high PA responses from the used QDs lies in the wavelength range of 620–645 nm, which is close to the NIR window transparency of biological tissues (650–950 nm), where interference with blood absorption is minimal 17. Progress in the development of NIR fluorescent QDs with absorption in the range of 750 nm and even 850 nm 2,18 opens up opportunities to use them also with PA/PT techniques.

The advantage of QDs in fluorescent applications is the possibility to use one optical source to excite QDs with different emission wavelengths (colors). This does not have a direct analogy in the utilized PT/PA techniques. Nevertheless, we recently developed time-resolved multispectral PA detection of nanoparticles with different absorption spectra 19, and this can thus provide a platform to use QDs as multicolor PA/PT contrast agents.

Currently, the time-resolved pump-probe PTI and PT thermolens technique operates more effectively in trans-illumination (forward) mode, which can provide imaging and detection of QDs in relatively transparent structures such as cells in suspension *in vitro*, and small-animal mesentery/ear models, as well as whole organisms such as Zebrafish and *C. elegans in vivo*. The PA schematic is more universal and can provide measurements both in forward and backward mode (i.e., laser and transducer are on one side), which is crucial for use *in vivo* on animal model and potentially on humans.

In summary, we herein demonstrated that QDs, in addition to being excellent fluorescent probes, can also be considered as PA and PT diagnostic probes, as well as PT sensitizers in nanotherapeutic applications. This observation may significantly extend the traditional application of QDs. Furthermore, the combination of QDs with PT/PA techniques that have inherent scattering and autofluorescent backgrounds 8,9,11 extends the applications of these

techniques themselves. Indeed, detection of both fluorescent light and heat can increase the diagnostic value of integrated PT-PA–fluorescence modalities. For example, *in vivo* studies could now be suggested that analyze QD pharmokinetics (e.g., clearance and accumulation rates, tissue biodistribution) in blood, the lymphatic system as well as tissues and organs up to 2–3 cm deep that are accessible with PA techniques 9; studies using fluorescent/PT/PA imaging for guiding PT therapy, including tracking of individual tumor cells, bacteria or adenoviruses labeled both with QDs and/or gold nanoparticles 10,13,20; mapping of tumor, sentinel lymph nodes and infected sites with integrated imaging modalities, or the use for multimodal molecular targeting and imaging in *in vivo* blood and lymph flow cytometry 5,6,16,19.

Acknowledgements

This work was supported by the National Institutes of Health/National Institute of Biomedical Imaging and Bioengineering under grants EB000873 and EB0005123, and by the Arkansas Biosciences Institute. The authors thank Dmitri Lapotko for help with building the PT microscope, which was further modified in this work.

References

1. Michalet X, Pinaud FF, Bentolila LA, Tsay JM, Doose S, Li JJ, Sundaresan G, Wu AM, Gambhir SS, Weiss S. Science 2005;307(5709):538–44. [PubMed: 15681376]
2. Lin S, Xie X, Patel MR, Yang YH, Li Z, Cao F, Gheysens O, Zhang Y, Gambhir SS, Rao JH, Wu JC. BMC Biotechnol 2007;7:67. [PubMed: 17925032]
3. Zharov VP, Lapotko D. Rev Sci Instrum 2003;74:785–788.
4. Berciaud S, Cognet L, Lounis B. Nano Lett 2005;5(11):2160–3. [PubMed: 16277445]
5. Zharov VP, Galanzha EI, Shashkov EV, Khlebtsov NG, Tuchin VV. Opt Lett 2006;31(24):3623–5. [PubMed: 17130924]
6. Zharov VP, Galanzha EI, Shashkov EV, Kim JW, Khlebtsov NG, Tuchin VV. J Biomed Opt 2007;12 (5):051503. [PubMed: 17994867]
7. Leatherdale CA, Woo WK, Mikulec FV, Bawendi MG. J Phys Chem B 2002;106(31):7619–7622.
8. Zharov VP, Lapotko D. IEEE J Sel Topics Quant Electron 2005;11:733–751.
9. Xu M, Wang LV. Review of Scientific Instruments 2006;77(4):041101.
10. Kim JW, Shashkov EV, Galanzha EI, Kotagiri N, Zharov VP. Lasers Surg Med 2007;39(7):622–34. [PubMed: 17868103]
11. Zharov, VP.; Letokhov, VS. Laser Optoacoustic Spectroscopy. Springer-Verlag; Berlin Heidelberg New York: 1986.
12. Pustovalov V, Smetannikov A, Zharov VP. Laser Phys Lett 2008;5:775–792.
13. Zharov VP, Kim JW, Curiel DT, Everts M. Nanomedicine 2005;1(4):326–345. [PubMed: 17292107]
14. Nikoobakht B, Burda C, Braun M, Hun M, El-Sayed MA. Photochem Photobiol 2002;75(6):591–7. [PubMed: 12081320]
15. Yong KT, Qian J, Roy I, Lee HH, Bergey EJ, Tramposch KM, He S, Swihart MT, Maitra A, Prasad PN. Nano Lett 2007;7(3):761–5. [PubMed: 17288490]
16. Bateman RM, Hodgson KC, Kohli K, Knight D, Walley KR. J Biomed Opt 2007;12(6):064005. [PubMed: 18163821]
17. Roggan A, Friebel M, Dorschel K, Muller AH. J Biomed Opt 1999;4(1):36–46.
18. Kim S, Lim YT, Soltesz EG, De Grand AM, Lee J, Nakayama A, Parker JA, Mihaljevic T, Laurence RG, Dor DM, Cohn LH, Bawendi MG, Frangioni JV. Nat Biotechnol 2004;22(1):93–7. [PubMed: 14661026]
19. Galanzha EI, Shashkov EV, Tuchin VV, Zharov VP. Cytometry A. 2008
20. Saini V, Martyshkin DV, Mirov SB, Perez A, Perkins G, Ellisman MH, Towner VD, Wu H, Pereboeva L, Borovjagin A, Curiel DT, Everts M. Small 2008;4(2):262–269. [PubMed: 18200644]

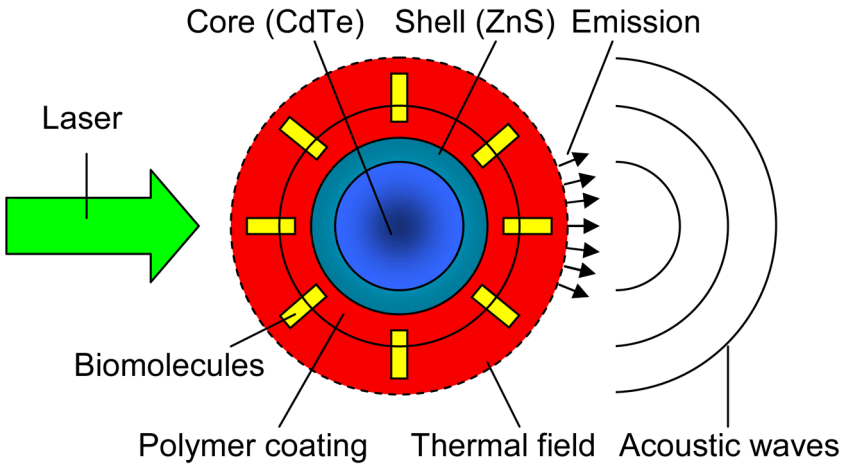

Figure 1.
Quantum dots as multimodal contrast agents for integrated fluorescent, photothermal, and photoacoustic detection.

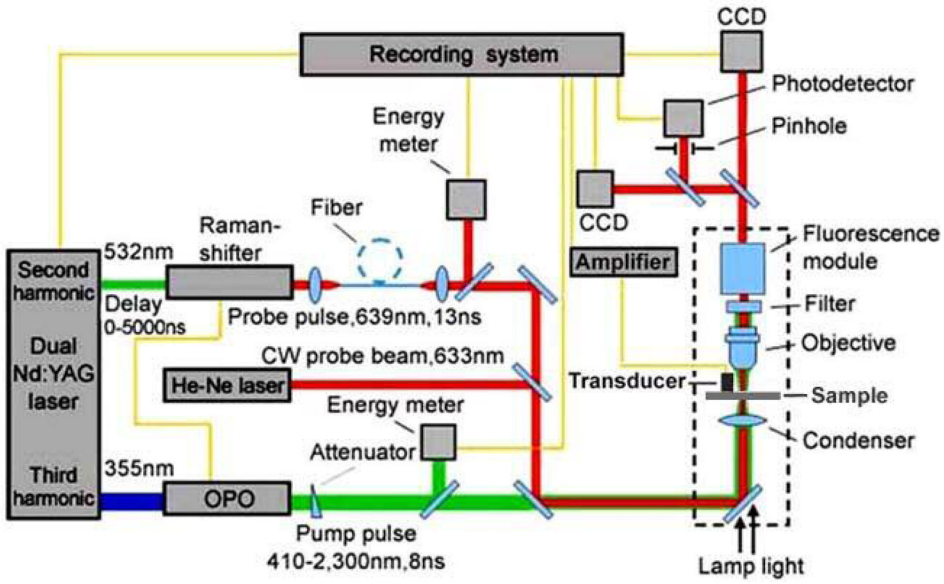

Figure 2.
Integrated laser microscope with PA, PT, and fluorescence modules.

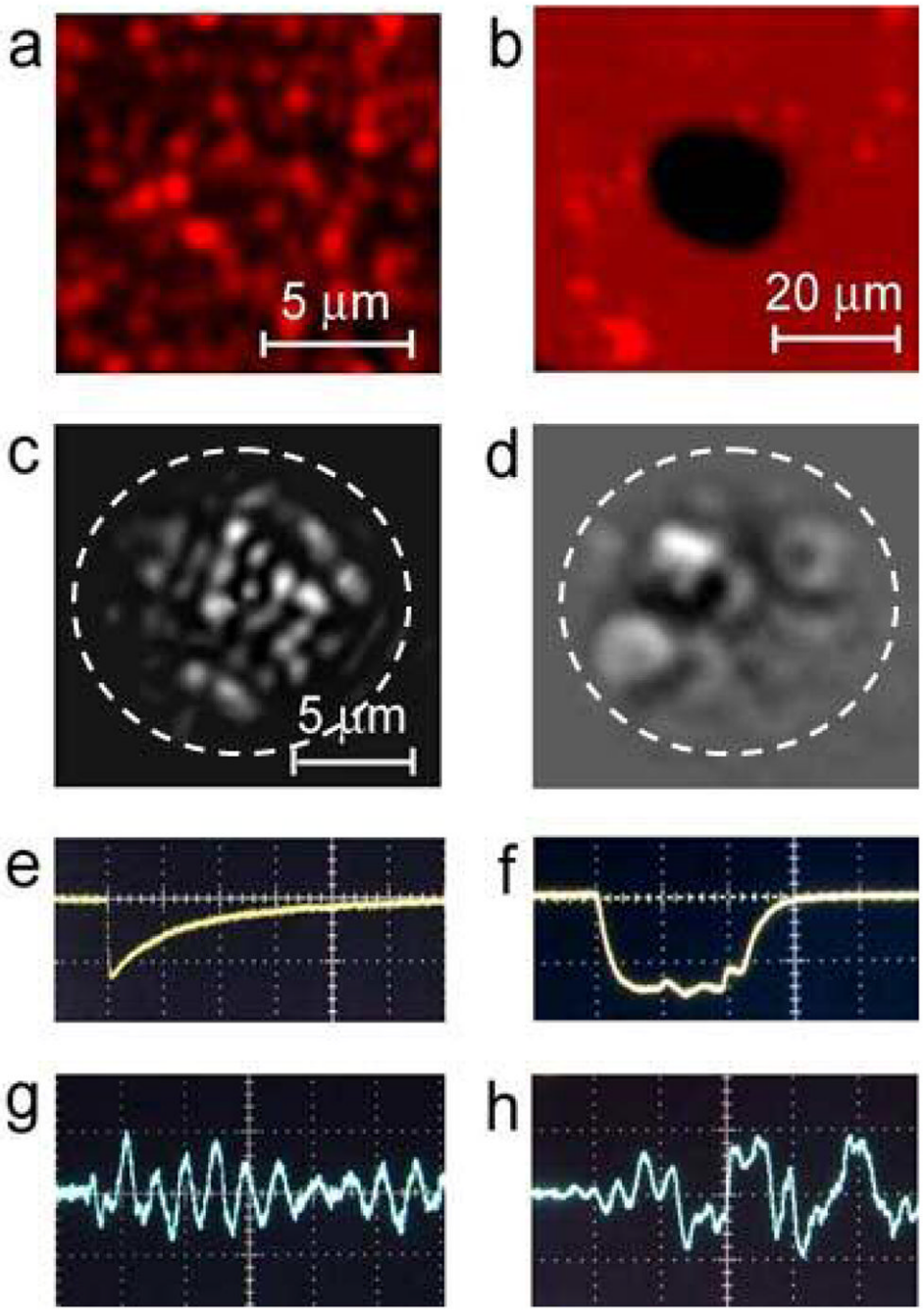

Figure 3.

High (a, 60 x) and low (b, 10 x) resolution fluorescence images of QDs before (a) and after (b) one laser pulse (532 nm, 3.5 J/cm^2, 20 μm diameter beam); excitation: 465 nm, emission: 665 nm. Note: the higher concentration of QDs and lower optical resolution in (b) do not allow to distinguish single QDs (just a few large clusters) compared to that of (a). PT images (c, d), PT thermolens signals (e–f), and PA signals (g,h) from QDs obtained with a single laser pulse (560 nm) at low (a,c,e,g) and high (b,d,f,h) laser fluence (0.6 J/cm and 3.5 J/cm^2, respectively). PT (c) and fluorescent (a) images were obtained from different parts of the same sample. Dash curve in (d) indicates laser beam diameter.

The time delay between pump and probe laser pulses [8] was (c) 10 ns, and (d) 150 ns. Amplitude (vertical axis), time scale (horizontal axis) (e) 100 mV, 40 μs/div; (f) 500 mV, 2μs/div; (g) 100 mV, 2 μs/div, (h) 500 mV, 2 μs/div.

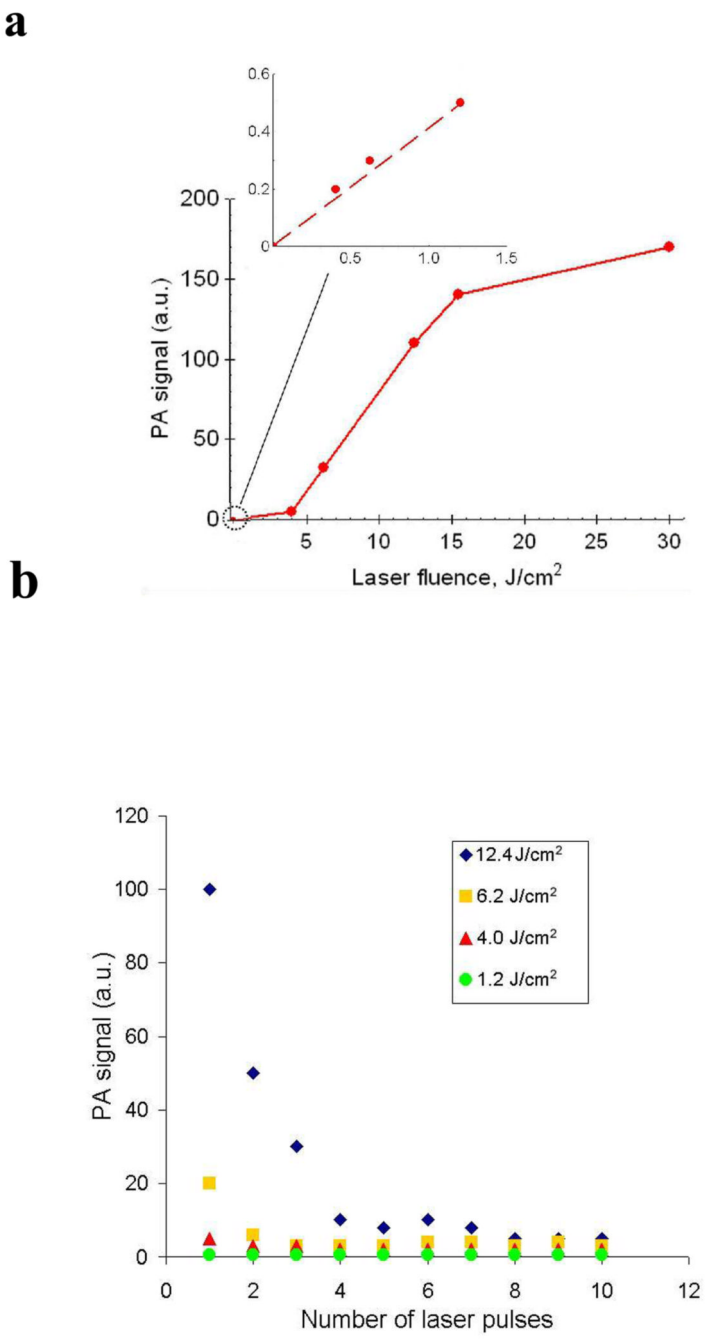

Figure 4.

(**a**) PA signal amplitudes from QDs as a function of laser fluence after one pulse. (**b**) PA signal amplitude from QDs as function of laser pulse number at various laser fluences: 12.4 (filled blue diamond), 6.2 J/cm^2 (filled yellow square), 4.0 J/cm^2 ((filled red triangle) and 1.2 J/cm^2 (filled green circles). Laser wavelength was 560 nm.

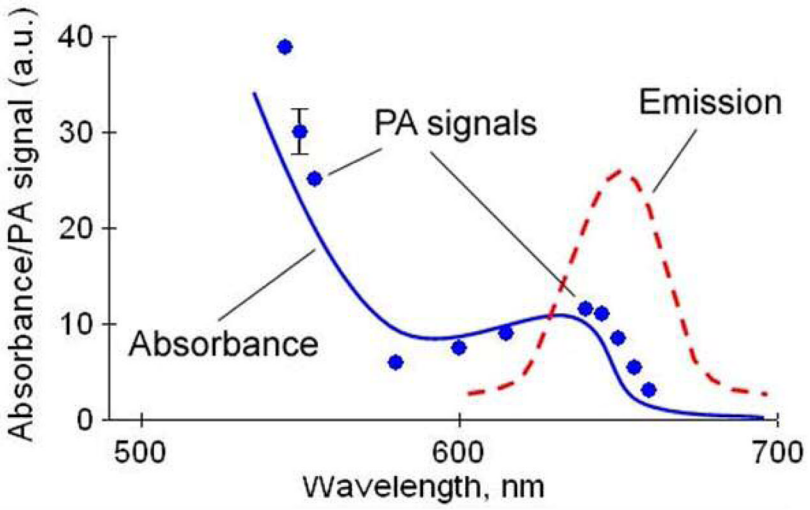

Figure 5.

Conventional absorption spectra (solid blue curve) and emission spectra of QDs (dash red curve) provided by manufacturers. PA spectra of QDs (thin slide with water suspension) with PA signal amplitude as a function of laser wavelength at one laser pulse, fluence 1.2 J/cm^2. PA spectra were normalized on the maximal absorption of conventional spectra at the wavelength 635 nm.